Next-generation all-solid-state battery (#ASSB)

Tuan Vo[a,b †], Claas Hüter[b], Stefanie Braun[a], Manuel Torrilhon[a]

[a]Department of Mathematics, Applied and Computational Mathematics (ACoM), RWTH Aachen University, Schinkelstraße 02, 52062 Aachen, Germany
[b]Institute of Energy and Climate Research (IEK-2), Forschungszentrum Jülich, Wilhelm-Johnen-Straße, 52428 Jülich, Germany

Mathematical modelling for the next-generation All-solid-state batteries: Nucleation (SE|SSE)$^{(*)}$-interface

Rechargeable Lithium-ion battery (LIB) is at the heart of every electric vehicle (EV), portable electronic device, and energy storage system [1]. Nowadays, LIBs enable human life more efficient and help to solve global environment issues thanks to EVs' zero emission. However, conventional LIB (c-LIB) is sensible to temperature and pressure, hence, flammable and explosive, which is undesirable. This bottleneck is mainly due to liquid-based electrolyte found in c-LIBs.

All-solid-state battery (ASSB) is one of promising candidates to overcome bottlenecks of c-LIBs. Thanks to solid-state electrolyte (SSE), ASSB is highly stable towards temperature and pressure. Nevertheless, Li-metal dendrite triggered at (SE|SSE)-interface [5] is the main drawback of ASSB since these dendritic threads extrapolate into SSE grain boundary network, causing crevice, degradation of ionic conductivity, and the probability of short-circuit, which is unfavorable.

Next-generation All-solid-state battery (ng-ASSB) with a consideration of nucleation criterion defined by

$$a_{\text{Griffith}} := a^* = \arg\min_{a\in\mathbb{R}} \iiint_\Omega f(a, \boldsymbol{u}, \theta; \lambda, \mu, \boldsymbol{d}^R \otimes \boldsymbol{d}^R)\, d\Omega - \iint_\Gamma f(a;\gamma)\, d\Gamma \Big|_{\boldsymbol{u}^{(s)}}$$

where $\boldsymbol{u}$ displacement field, θ temperature field, a crevice length, λ, μ Lamé constants, $\boldsymbol{d}^R \otimes \boldsymbol{d}^R$ embedded misorientation structural tensor, and γ cracking-surface energy density, can help to improve ASSB performance.

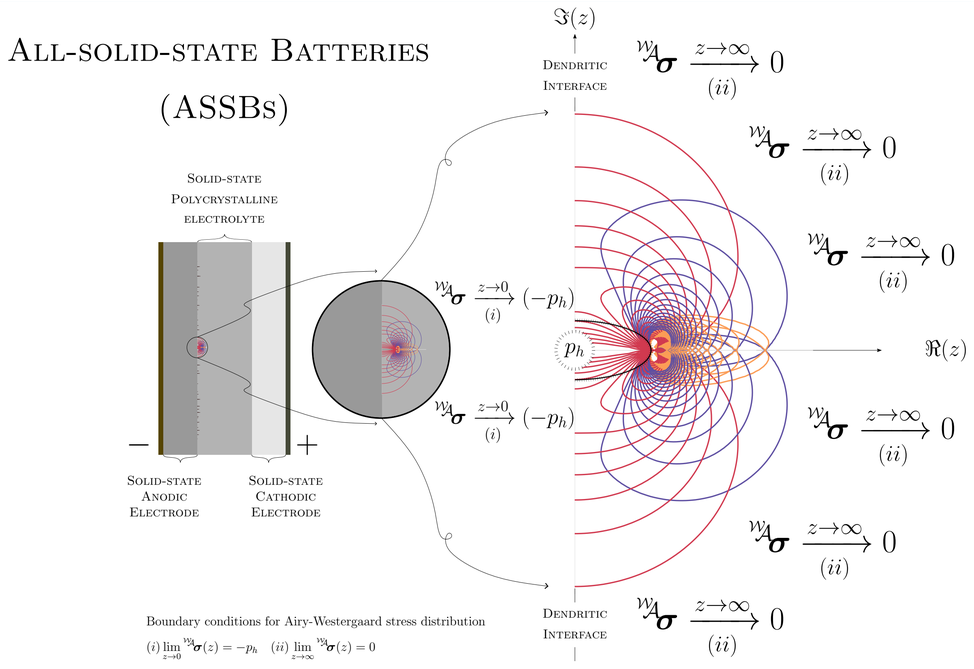

Interface Analysis

Interface between solid electrode and solid-state electrolyte (SE|SSE) taking place at space charge layer (SCL) [2] found in ASSBs critically exhibits mechanical and electrochemical instability [3]. This evidence points directly to the fact that the soft metallic li anode is erroneously prone to triggering dendrites, under cycles of electric charge & discharge [5].

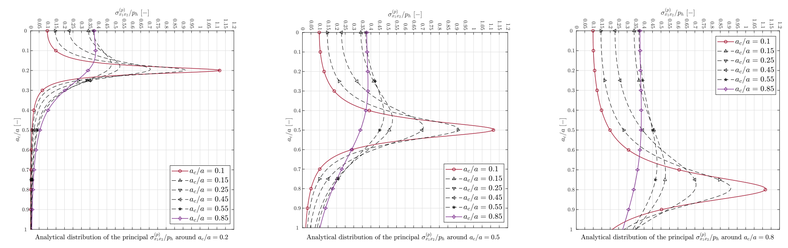

Distribution: ana. max. shear stress ${}^{w_A}\sigma\Pi_{x_1x_2}$ around crack tip a_c.

Next-generation All-solid-state battery

Nucleation criterion governs the instable (SE|SSE)-interface [3]

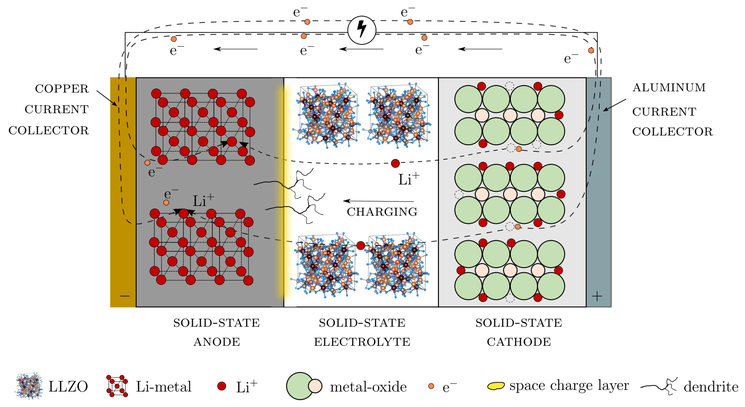

✓ **Thermodynamic consistency** is satisfied, followed by [2].
✓ **Closure** $\bar{\Omega}$ is fulfilled by 15 moments, followed by [4].

Embedded structural-tensor in SSE

Polycrystalline garnet-type SSE [5] such as LLZO exhibit grain boundary network, and grains with variation of {size, shape} under microscopic observation. Hence, this microstructure is potentially prone to nuances of destruction.

$\boldsymbol{M} = \boldsymbol{d}^R_{G_1} \otimes \boldsymbol{d}^R_{G_2}$ given by $\mathbb{G} := \{\boldsymbol{Q}_{||_d}, \boldsymbol{Q}_{\perp_d}\} \subset \mathcal{O}(3)$.

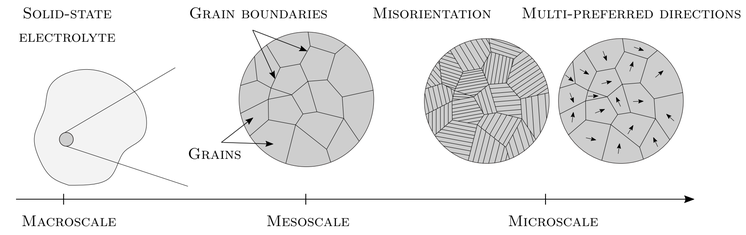

Consequentially, dendrites contribute to degradation of ionic conductivity and tiny-cracks tracing along grain boundaries.

Nucleation interface: Taking place at the critical dendritic interface

Coupled fields: Displacement field $\boldsymbol{u}$ and temperature field θ; structural tensor $\boldsymbol{M}$

$$\boldsymbol{u} : \begin{cases} \Omega \times \mathbb{R}_+ \to \mathbb{R}^3, \\ (\boldsymbol{x}, t) \mapsto \boldsymbol{u}(\boldsymbol{x}, t), \end{cases} \quad \theta : \begin{cases} \Omega \times \mathbb{R}_+ \to \mathbb{R}, \\ (\boldsymbol{x}, t) \mapsto \theta(\boldsymbol{x}, t), \end{cases} \quad \boldsymbol{M}^{\{RR,RE\}}_{i=1,\dots,N} : \begin{cases} \boldsymbol{d}^R_{\text{Grain i}} \otimes \boldsymbol{d}^R_{\text{Grain i}} \\ \boldsymbol{d}^R_{\text{Grain i}} \otimes \boldsymbol{d}^E \end{cases}$$

Governing conservation equations

$$\frac{d}{dt}\int_\Omega (\cdot)\, d\Omega = \int_\Omega (\cdot)^{\text{action}}\, d\Omega + \int_{\partial\Omega} (\cdot)^{\text{action}}\, d\partial\Omega + \int_\Omega (\cdot)^{\text{production (+/-)}}\, d\Omega$$

$\rho(\boldsymbol{x}, t)$ is mass density per unit volume (puv); $\boldsymbol{b}(\boldsymbol{x}, t)$ body force puv; $\boldsymbol{v}(\boldsymbol{x}, t)$ velocity; $e(\boldsymbol{x}, t)$ internal energy puv; $\boldsymbol{q}(\boldsymbol{x}, t)$ heat flux; $r(\boldsymbol{x}, t)$ heat source puv; $\boldsymbol{\sigma}$ Cauchy stress and $\boldsymbol{\varepsilon}$ infinitesimal strain. Helmholtz energy functional

$$a_{\text{Griffith}} := a^* = \arg\min_{a\in\mathbb{R}} \iiint_\Omega f(a, \boldsymbol{u}; \lambda, \mu, \boldsymbol{d} \otimes \boldsymbol{d})\, d\Omega - \iint_\Gamma f(a;\gamma)\, d\Gamma \Big|_{\boldsymbol{u}^{(s)}}$$

Governing partial differential equation (PDE) of deformation takes the form

$$\partial_t \boldsymbol{u} + \nabla \cdot \left(\overset{4}{\mathbb{C}} f_{\text{alocation}}(\lambda, \mu, \boldsymbol{d}^R_{G_i, i=1,\dots,N}, \boldsymbol{d}^E; \boldsymbol{x}) : \nabla \boldsymbol{u}^{(s)} \right) + \rho \boldsymbol{b} = -\rho \nabla V_e,$$

where $V_e : \mathbb{R}^3 \to \mathbb{R}$ is the uniform electric potential applied globally on ASSB.

Strain energy: Interface between solid electrode and solid-state electrolyte (SE|SSE) taking place at space charge

$$\iiint_\Omega f(a, \boldsymbol{u}; \lambda, \mu, \boldsymbol{d} \otimes \boldsymbol{d})\, d\Omega$$

Surface energy: Interface between solid electrode and solid-state electrolyte (SE|SSE) taking place

$$\iint_\Gamma f(a;\gamma)\, d\Gamma$$

Therefore, the governing problem of dendritic nucleation at (SE|SSE) takes the form

$$\partial_t \bar{\boldsymbol{u}} + \nabla \cdot \left(\overset{4}{\mathbb{C}} f_{\text{alocation}}(\lambda, \mu, \boldsymbol{d}^R_{G_i, i=1,\dots,N}, \boldsymbol{d}^E; \boldsymbol{x}) : \nabla \boldsymbol{u}^{(s)} \right) + \rho \boldsymbol{b} = -\rho \nabla V_e, \quad (1)$$

$$\text{s.t.} \quad a_{\text{Griffith}} := a^* = \arg\min_{a\in\mathbb{R}} \iiint_\Omega f(a, \boldsymbol{u}, \theta; \lambda, \mu, \boldsymbol{d} \otimes \boldsymbol{d})\, d\Omega - \iint_\Gamma f(a;\gamma)\, d\Gamma \Big|_{\bar{\boldsymbol{u}}} \quad (2)$$

where deformation $\bar{\boldsymbol{u}}$ is (i) based on (1), and then (ii) for *Griffith*-analysis in (2).

Boundary conditions

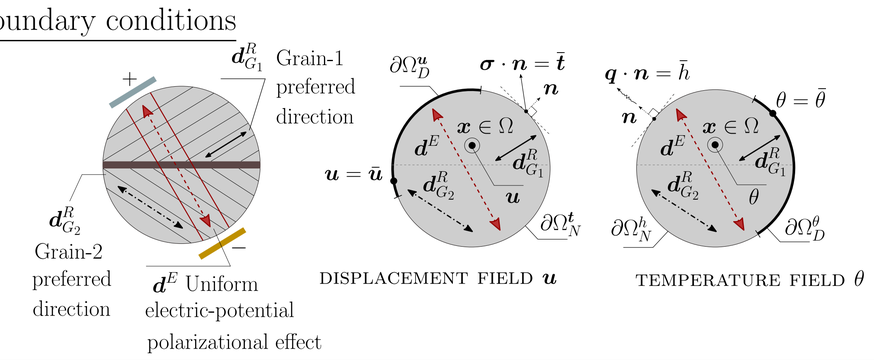

Numerical spectral of *Griffith* criterion in x-direction at (SE|SSE) yields

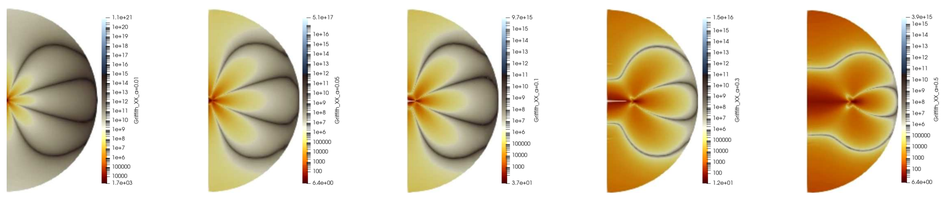

(a) Case 1 $a_{\text{crevice}} = 0.01$ (b) Case 2 $a_{\text{crevice}} = 0.05$ (c) Case 3 $a_{\text{crevice}} = 0.1$ (d) Case 4 $a_{\text{crevice}} = 0.3$ (e) Case 5 $a_{\text{crevice}} = 0.5$

where a sample of 5 cases with various prescribed crevice length is studied.

FEM: Strain energy density

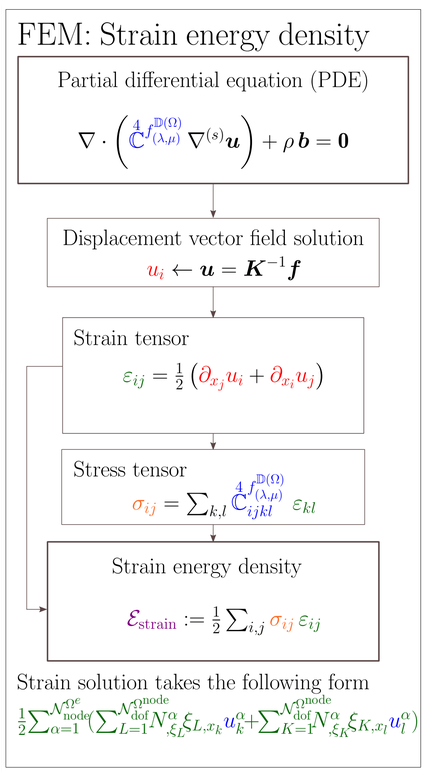

Strain solution takes the following form

$$\frac{1}{2}\sum_{\alpha=1}^{\mathcal{N}^{\Omega^e}_{\text{node}}} \left(\sum_{L=1}^{\mathcal{N}^{\Omega^{\text{node}}}_{\text{dof}}} N^\alpha_{,\xi_L} \xi_{L,x_k} u^\alpha_k + \sum_{K=1}^{\mathcal{N}^{\Omega^{\text{node}}}_{\text{dof}}} N^\alpha_{,\xi_K} \xi_{K,x_l} u^\alpha_l \right)$$

Analysis: Airy-Westergaard function used for stress analysis: (i) max. shear stress and (ii) principal stresses

$${}^{w_A}\mathcal{A} : \begin{cases} \mathbb{C} \to \mathbb{C}, \\ z \mapsto {}^{w_A}\mathcal{A}(z) := \Re\left(\oiint_\Gamma \mathcal{K}^{(\star)}\, dz \right) + x_2\, \Im\left(\oint_\Gamma \mathcal{K}^{(\star)}\, dz \right), \end{cases} \quad \mathcal{K}^{(\star)} : \begin{cases} \mathbb{C} \to \mathbb{C}, \\ z \mapsto \mathcal{K}^{(\star)} := -p_h + p_h / \sqrt{1 - a^2/z^2}, \end{cases}$$

where a the crevice length, p_h pressure at the opening crevice on dendritic interface, and $\forall\, \{p_h, a\} \in \mathbb{R}_+$.

Numerics → FEM: element matrix $\boldsymbol{K}^e$ approx. by *Gauss quadrature*; indices imply $4 + 2 = 6$ *for-loop*:

$$K^{e\,\alpha\beta}_{ik} = \int_{\Omega^\xi} \left(\mathcal{L}^\alpha_1\, \mathbb{C}^{fGL}_{i1k1}(\boldsymbol{x})\, \mathcal{R}^\beta_1 + \mathcal{L}^\alpha_1\, \mathbb{C}^{fGL}_{i1k2}(\boldsymbol{x})\, \mathcal{R}^\beta_2 + \mathcal{L}^\alpha_2\, \mathbb{C}^{fGL}_{i2k1}(\boldsymbol{x})\, \mathcal{R}^\beta_1 + \mathcal{L}^\alpha_2\, \mathbb{C}^{fGL}_{i2k2}(\boldsymbol{x})\, \mathcal{R}^\beta_2 \right) \det(\boldsymbol{J})\, d\Omega^\xi$$

where $\mathcal{L}^\alpha_j$ and $\mathcal{R}^\beta_l$ are gradients of basis functions at node α^{th} and β^{th}, respectively.

Contact

Tuan Vo
vo@acom.rwth-aachen.de

Scan me

References

[1] **T.Vo**, *Modeling the swelling phenomena of li-ion batt. cells based on a numerical chemo-mech. coupled approach.* MA, Robert Bosch Battery Systems GmbH, **2018**.

[2] **S.Braun**, C.Yada and A.Latz, *Thermodynamically consistent model for Space-Charge-Layer formation in a solid electrolyte.* Jr. Phys. Chem., 119, 22281-22288, **2015**.

[3] **C.Hüter**, S.Fu, M.Finsterbusch, E.Figgemeier, L.Wells, and R.Spatschek, *Electrode-electrolyte interface stability in solid state electrolyte system: influence of coating thickness under varying residual stresses.* AIMS Materials Science, 4(4):867-877, **2017**.

[4] **M.Torrilhon**. *Modeling nonequilibrium gas flow based on moment equations.* Annual Review of Fluid Mechanics, 48(1):429-458, **2016**.

[5] **S.Kim**, J.S.Kim, L.Miara, Y.Wang, S.K.Jung, S.Y.Park, Z.Song, H.King, M.Badding, J.M.Chang, V.Roev, G.Yoon, R.Kim, J.H.Kim, K.Yoon, D.Im, and K.Kang, *High-energy and durable li metal batt. using garnet-type solid electrolytes with tailored li-metal compatibility.* Nature Communications, 13(1):1883, **2022**.

Society for Industrial and Applied Mathematics
siam 2023 Conference on Computational Science and Engineering AMSTERDAM
Applied and Computational Mathematics
RWTH AACHEN UNIVERSITY
JÜLICH Forschungszentrum